AGU PUBLICATIONS

JGR

Journal of Geophysical Research: Earth Surface

RESEARCH ARTICLE
10.1002/2014JF003323

Key Points:
- High relative roughness alone causes increased threshold shear stress in rivers
- Changes in the velocity distribution control the onset of motion in shallow flow
- Nondimensional stream power is a more consistent predictor of sediment transport

Correspondence to:
J. P. Prancevic,
jprancev@caltech.edu

Citation:
Prancevic, J. P., and M. P. Lamb (2015), Unraveling bed slope from relative roughness in initial sediment motion, *J. Geophys. Res. Earth Surf.*, *120*, 474–489, doi:10.1002/2014JF003323.

Received 25 AUG 2014
Accepted 21 JAN 2015
Accepted article online 26 JAN 2015
Published online 14 MAR 2015

Unraveling bed slope from relative roughness in initial sediment motion

Jeff P. Prancevic[1] and Michael P. Lamb[1]

[1]Division of Geological and Planetary Sciences, California Institute of Technology, Pasadena, California, USA

Abstract Understanding incipient sediment transport is crucial for predicting landscape evolution, mitigating flood hazards, and restoring riverine habitats. Observations show that the critical Shields stress increases with increasing channel bed slope, and proposed explanations for this counterintuitive finding include enhanced form drag from bed forms, particle interlocking across the channel width, and large bed sediment relative to flow depth (relative roughness). Here we use scaled flume experiments with variable channel widths, bed slopes, and particle densities to separate these effects which otherwise covary in natural streams. The critical Shields stress increased with bed slope for both natural gravel ($\rho_s = 2.65$ g/cm^3) and acrylic particles ($\rho_s = 1.15$ g/cm^3), and adjusting channel width had no significant effect. However, the lighter acrylic particles required a threefold higher critical Shields stress for mobilization relative to the natural gravel at a fixed slope, which is unexpected because particle density is accounted for directly in the definition of Shields stress. A comparison with model predictions indicates that changes in local velocity and turbulence associated with increasing relative roughness for lighter materials are responsible for increasing the critical Shields stress in our experiments. These changes lead to concurrent changes in the hydraulic resistance and a nearly constant critical stream power value at initial motion. Increased relative roughness can explain much of the observed heightened critical Shields stresses and reduced sediment transport rates in steep channels and also may bias paleohydraulic reconstructions in environments with exotic submerged densities such as iron ore, pumice, or ice clasts on Titan.

1. Introduction

Predicting sediment transport in steep, shallow flows is of fundamental importance to several problems within Earth and planetary sciences: mitigating hazards from debris-laden floods [e.g., *Prancevic et al.*, 2014], landscape evolution [e.g., *Howard*, 1994; *Tucker and Slingerland*, 1997], and Earth and planetary paleoflood reconstructions [e.g., *Costa*, 1983; *Perron et al.*, 2006]. For example, landscape evolution is driven by river incision, which, in turn, is sensitive to the onset of sediment motion [e.g., *Howard*, 1994; *Tucker and Slingerland*, 1997]. Studies show that normalized channel steepness in natural catchments is consistent with observed erosion rates only when thresholds for sediment motion are applied [e.g., *Lague*, 2003; *Dibiase and Whipple*, 2011]. Initial sediment motion is usually cast in terms of the bed stress normalized by grain weight per unit bed area, or Shields stress:

$$\tau^* = \frac{\tau_b}{(\rho_s - \rho)gD}, \tag{1}$$

where τ_b is the spatially and temporally averaged basal shear stress, g is gravitational acceleration, D is the median grain diameter, ρ_s is sediment density, and ρ is fluid density. The Shields stress at initial sediment motion, or critical Shields stress (τ_c^*), is sediment-size dependent but has been shown to equal a constant value between about 0.03 and 0.06 for high particle Reynolds numbers ($Re_p > 10^2$) typical of gravel and coarser sediment [e.g., *Buffington and Montgomery*, 1997]. Theoretical models that balance fluid forces and the frictional stability of grains support this finding [e.g., *Wiberg and Smith*, 1987].

Surprisingly, field and flume studies with steeper bed slopes reveal that sediment of a given size requires higher Shields stresses for mobilization despite the increased magnitude of gravity acting on the grains in the downstream direction [*Ashida and Bayazit*, 1973; *Bathurst et al.*, 1984; *Mueller et al.*, 2005; *Gregoretti*, 2008; *Bunte et al.*, 2013; *Scheingross et al.*, 2013; *Prancevic et al.*, 2014]. Several different mechanisms have been proposed to explain this counterintuitive observation, but few have been isolated because all tend to covary with channel slope in natural streams. For example, steep channels tend to have channel widths (W) that are

narrow relative to sediment size (e.g., $W/D < 10$), and this may cause high τ_c^* due to particle force chains that span the channel width (i.e., a jammed state [*Zimmermann et al*., 2010]) and due to increased momentum loss through wall drag [e.g., *Buffington and Montgomery*, 1999]. Steep channels also often contain large bed forms and immobile boulders, which extract momentum from the flow, reduce the basal shear stress available to move sediment, and therefore might cause higher than expected values of τ_c^* [e.g., *Zimmermann and Church*, 2001; *Yager et al*., 2007].

Field and flume studies also show that flows over steep (>0.5°) erodible beds approach a critical Froude number ($Fr = \frac{U}{\sqrt{gH}}$, where U is the time-averaged and spatially averaged flow velocity and H is flow depth) [e.g., *Grant*, 1997]. Experiments measuring the drag on an individual hemisphere in shallow flow show that supercritical Froude numbers induce up to an order-of-magnitude decrease in the drag coefficient relative to subcritical cases [*Flammer et al*., 1970]. This effect could increase τ_c^* in steep channels. However, supercritical flows are rare in natural alluvial channels because of a coincident increase in frictional resistance with increasing slope. Observations of mean flow velocity indicate that the friction factor

$$C_f = \left(\frac{u^*}{U}\right)^2, \tag{2}$$

where $u^* = \left(\frac{\tau_b}{\rho}\right)^{1/2}$ is the shear velocity, increases sharply in steep, shallow flows [e.g., *Rickenmann and Recking*, 2011]. In other studies researchers have observed that high relative roughness (i.e., D/H), typical of steep channels, causes changes in velocity profiles [e.g., *Bayazit*, 1976; *Nikora et al*., 2001] and near-bed turbulence intensity [*Bayazit*, 1976; *Carollo et al*., 2005], both of which may lead to heightened τ_c^* [*Shields*, 1936; *Aksoy*, 1973; *Bettess*, 1984; *Vollmer and Kleinhans*, 2007; *Lamb et al*., 2008; *Recking*, 2009] and heightened C_f.

As an alternative to critical Shields stress, several researchers have advocated the use of unit stream power ($\omega = \tau_b U$) to predict sediment transport [*Bagnold*, 1980; *Ferguson*, 2005; *Parker et al*., 2011; *Ferguson*, 2012]. Stream power is a particularly convenient parameter for landscape-scale studies of erosion [e.g., *Howard*, 1994; *Whipple and Tucker*, 1999], where flow discharge is more easily approximated than flow depth by virtue of the scaling between discharge and drainage area [e.g., *Hack*, 1957]. *Ferguson* [2005] proposed that the critical unit stream power needed to initiate sediment transport should be lower in steep channels due to the increased component of gravity in the downstream direction. A subsequent analysis of field and flume data [*Parker et al*., 2011] instead indicates that the nondimensional critical stream power,

$$\omega_c^* = \frac{\omega_c}{g(\rho_s - \rho)\sqrt{RgD^3}}, \tag{3}$$

is a constant of $\omega_c^* = 0.1$, independent of bed slope. A revised theoretical model by *Ferguson* [2012] included a slope-dependent critical Shields stress and arrived at a similar prediction for critical unit stream power, $\omega_c^* \sim 0.1$, for bed slope angles smaller than ~5°. These findings indicate that changes in the critical Shields stress and flow resistance are interrelated as both depend on relative roughness, although a mechanistic rationale for this has not been established.

In a series of recent theoretical models, relative roughness has emerged as the leading hypothesis behind the heightened τ_c^* with increasing channel slope [*Lamb et al*., 2008; *Recking*, 2009; *Ferguson*, 2012]. However, testing this theory is challenging because channel slope, channel width, bed forms, Froude number, and relative roughness covary in natural channels. Although flume experiments offer an opportunity to separate their effects on initial sediment motion, few experimental studies have been conducted on incipient motion at very steep bed slopes (>5°) [*Bayazit*, 1976; *Fernandez Luque and Van Beek*, 1976; *Chiew and Parker*, 1994; *Gregoretti*, 2008; *Prancevic et al*., 2014]. Of these studies, most confirm that steeper channel beds lead to heightened critical Shields stresses. However, no studies in steep channels separate the naturally covarying factors of relative roughness and channel slope [*Ashida and Bayazit*, 1973; *Bathurst et al*., 1984; *Bettess*, 1984; *Shvidchenko and Pender*, 2000; *Prancevic et al*., 2014]. Therefore, results from these studies cannot be used to test for the effect of relative roughness on τ_c^* independent of channel slope and Froude number.

In contrast, initial motion experiments conducted in sealed ducts, which contain no free surface and therefore no change in relative roughness or Froude number effects, show that τ_c^* decreases with increasing

bed slope [*Fernandez Luque and Van Beek*, 1976; *Chiew and Parker*, 1994], consistent with classic theory [*Wiberg and Smith*, 1987], and opposite to observations in natural channels. These duct experiments suggest that heightened critical Shields stress cannot be explained in the absence of a water free surface. Open-channel flow experiments have yet to be conducted, however, to test whether heightened critical Shields stress can be explained by high relative roughness in the absence of steep channel slopes, particle interlocking, and bed form-induced form drag. This is our goal.

2. Experimental Design and Rationale

The experiments were designed as tests of recent theoretical models for initial sediment motion by isolating the effect of relative roughness from channel slope, Froude number, form drag due to bed forms, and particle jamming and interlocking across the channel width (Table 1). Of these factors, the most difficult to separate are channel slope and relative roughness. This can be illustrated by rewriting equation (1) for initial sediment motion in steady and uniform open-channel flow as

$$\tau_c^* = \frac{H_c \sin\theta}{RD}, \tag{4}$$

where $R = \frac{(\rho_s - \rho)}{\rho}$ is the relative submerged density and θ is the inclination angle of the channel bed and water surface. Inspection of equation (4) shows that τ_c^* is the product of three dimensionless variables (H/D, $1/R$, and $\sin\theta$), and these must covary if τ_c^* is to remain constant over a wide range of channel conditions. In typical natural and experimental conditions, R is constant and relative roughness (D/H) therefore must covary with channel slope (θ) at initial motion if τ_c^* is constant. However, if τ_c^* varies with either θ or D/H, there will be an apparent dependence on both variables. It is clear from equation (4) that the only way to isolate the effects of relative roughness from channel slope in open-channel flow is by changing the submerged specific density of sediment (R). Changing the material density of the sediment results only in a change in the buoyant weight of the grain [e.g., *Archimedes*, 1897], which is already accounted for in the definition of τ_c^*. Indeed, previous studies have shown that at low slopes and small relative roughness, large changes in the relative submerged density ($R = 0.06$ to 6.9) have a negligible effect on the critical Shields stress [e.g., *Shields*, 1936; *White*, 1940]. However, in the steep, shallow flow regime, changing R at constant θ results in covarying changes in D/H, which may affect τ_c^*. Thus, submerged specific density is the key to testing the effect of relative roughness on τ_c^* independent of channel bed slope.

2.1. Experimental Setup

Here we build on the experiments of *Prancevic et al*. [2014], which measured the critical Shields stress of natural well-sorted, semiangular gravel ($D = 1.5$ cm; $\rho_s = 2.65$ g/cm^3; $R = 1.65$) over a wide range in channel slopes from $\theta = 1.8°$ to slopes steeper than the transition to mobilization by mass failure ($\theta > 22.3°$). To isolate relative roughness from channel slope, we conducted a series of complementary experiments using well-sorted, semiangular acrylic particles ($D = 2.3$ cm, $\rho_s = 1.15$ g/cm^3, $R = 0.15$). The acrylic particles were manufactured as spheres, and an initial set of experiments showed that initial sediment motion for perfect spheres was phenomenologically different from that of natural gravel (e.g., where sheets of particles translated together along planes of symmetry). To break the symmetrical packing, we heated and deformed the acrylic particles to create random, semiangular shapes similar to the natural gravel used in the experiments (Figure 1). Owing to their lower submerged density, the acrylic particles require substantially less basal shear stress (τ_b) to move in comparison to gravel. Thus, for a given channel slope, the acrylic particles move under much larger relative roughness than the gravel, allowing us to isolate the effect of relative roughness (smaller flow depth) on initial motion from channel slope by comparing the gravel and acrylic results. The particles are sufficiently large that the initial motion was particle Reynolds number (Re_p) and sediment size independent [*Shields*, 1936] (i.e., $Re_p > 10^3$, Table 1).

We attempted to eliminate particle jamming in our experiments by using smooth walls and wide channels relative to the grain diameter [e.g., *Zimmermann et al*., 2010]. To test whether particle jamming was occurring, experiments were conducted using two different channels widths for each material ($W/D = 23$ and 9 for gravel [*Prancevic et al*., 2014]; $W/D = 6$ and 4 for acrylic). We also performed an additional set of experiments with gravel using rough walls (with gravel glued to the walls) to further test for any jamming effects (Table 1).

Journal of Geophysical Research: Earth Surface 10.1002/2014JF003323

Table 1. Experimental Sets

Particle Material	Particle Relative Submerged Density, R	Median Particle Diameter, D (cm)	Flume Width, W (cm)	W/D	Wall Texture	Bed Slope Angle, θ (°)	Critical Shields Stress, τ_c^*	Critical Unit Discharge, q_{surf} (m^2/s)	Relative Roughness, D/H	Particle Reynolds Number at the Onset of Motion[a], Re_p	Froude Number at the Onset of Motion, Fr_c	Friction Factor, C_f
						Prancevic et al. [2014]						
Gravel	1.65	1.5	35	23	Smooth	1.9	0.036	0.0190	0.56	1400	1.38	0.018
						3.3	0.049	0.0173	0.71	1600	1.82	0.018
						5.6	0.063	0.0098	0.94	1900	1.57	0.040
						6.8	0.075	0.0079	0.96	2000	1.31	0.070
						8	0.08	0.0062	1.06	2100	1.19	0.100
						9.8	0.09	0.0056	1.16	2200	1.23	0.114
						12.4	0.1	0.0040	1.33	2300	1.08	0.188
						13.5	0.11	0.0036	1.32	2500	0.96	0.263
						15.6	0.12	0.0028	1.41	2600	0.82	0.413
Gravel	1.65	1.5	13	8.7	Smooth	5.9	0.062	0.0057	1.01	1800	1.01	0.101
						11.5	0.11	0.0039	1.12	2500	0.81	0.313
						14.2	0.12	0.0037	1.28	2600	0.94	0.288
						16.9	0.13	0.0021	1.42	2700	0.61	0.813
						19.6	0.16	0.0022	1.35	3000	0.60	1.000
						22.3[b]	0.21	0.0032	1.18	3400	0.71	0.813
						This Study						
Gravel	1.65	1.5	32	21	Rough	1.8	0.033	0.0182	0.58	1300	1.39	0.016
						3.1	0.048	0.0167	0.68	1600	1.65	0.020
						4.3	0.054	0.0126	0.84	1700	1.69	0.026
						5.6	0.058	0.0093	1.02	1800	1.67	0.035
						8	0.074	0.0065	1.15	2000	1.40	0.071
Acrylic	0.15	2.3	9	3.9	Smooth	0.7	0.058	0.0055	1.40	1000	0.84	0.018
						0.9	0.074	0.0057	1.42	1200	0.89	0.020
						1.4	0.11	0.0031	1.48	1400	0.51	0.093
Acrylic	0.15	2.3	13	5.7	Smooth	0.7	0.048	0.0047	1.70	900	0.94	0.014
						0.9	0.072	0.0031	1.45	1100	0.49	0.065
						1.4	0.11	0.0024	1.48	1400	0.40	0.150
						2.6[b]	0.19	0.0022	1.59	1800	0.41	0.275

[a]The particle Reynolds number is defined as $Re_p = (\tau^* RgD)^{1/2} D/\nu$, where ν is the kinematic viscosity.
[b]At the steepest slope tested for each material bed failure was observed, in addition to fluvial transport.

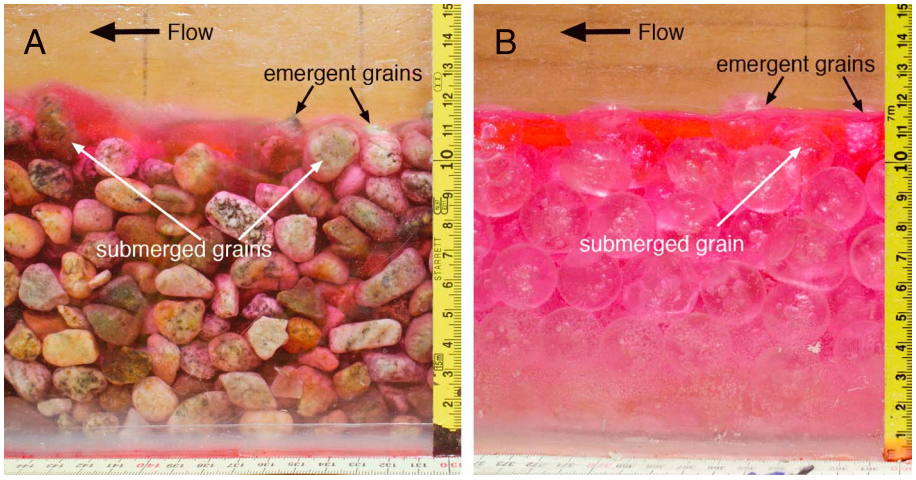

Figure 1. Photographs taken during (a) a gravel experiment at $\theta = 22.3°$ and (b) an acrylic experiment at $\theta = 2.6°$, showing some emergent grains, and others that remain submerged despite extending above the average water surface height.

To remove the stabilizing effect of bed forms (including morphologic form drag) on initial motion, all of our experiments started with a flat, hand-screed bed. Although initial water working can change initial motion criteria [e.g., *Kirchner et al.*, 1990], we found that step-pools and alternate bars formed rapidly in our experiments, and the only means to eliminate bed forms as variables was to start from a planar, unworked bed. In addition, we ceased the experiments when sediment transport significantly altered the bed from its initial state by building bed forms that were two grain diameters in relief or more.

We conducted 28 new experiments over a broad range of bed slopes ($\theta = 0.7°$ to $8.0°$) in a 5 m long tilting flume (Figure 2), the same as that used in *Prancevic et al.* [2014]. All experiments began with a planar loose bed, ~10.5 cm thick. The sediment bed was primarily composed of loose gravel. However, there was a single layer of fixed gravel at the base of loose material to prevent basal sliding of the entire bed. Also, the downstreammost section of the flume was protected from erosion due to water surface drawdown at the flume outlet using a 40 cm long fixed bed, also ~10.5 cm in thickness.

2.2. Measuring the Critical Shields Stress

We incrementally increased the water discharge, pausing for 3 to 12 min at each discharge for flow measurements and observations of sediment transport. Because our target was initial motion, no sediment was fed into the flume. We calculated the critical Shields stress using equation (4) and by making a low-slope approximation ($\sin\theta \approx \tan\theta$) to be consistent with previous work. Owing to the rough water surface in steep and shallow flows (Figure 1), point measurements of flow depth were difficult to collect and yielded considerable scatter. Instead, flow depth was calculated using conservation of mass ($H = q_{surf}/U$) and measurements of surface flow discharge per unit width (q_{surf}) and width- and depth-averaged flow velocity (U). The total discharge was measured using an inline flow meter, and surface flow discharge was determined by subtracting the saturated subsurface discharge (Figure 3). We defined the saturated subsurface discharge as that required to fully saturate the average thickness of the bed. To calculate these values, we mapped

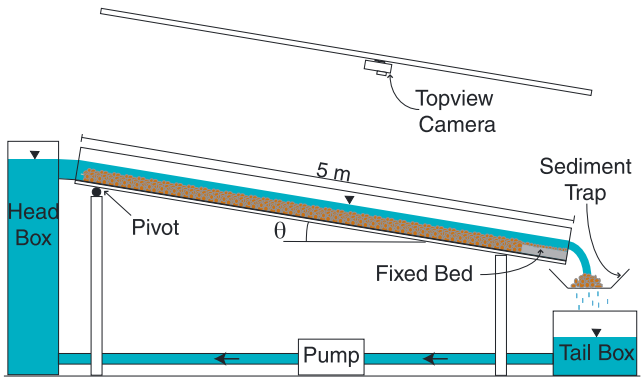

Figure 2. Flume schematic showing the general experimental setup. Not to scale.

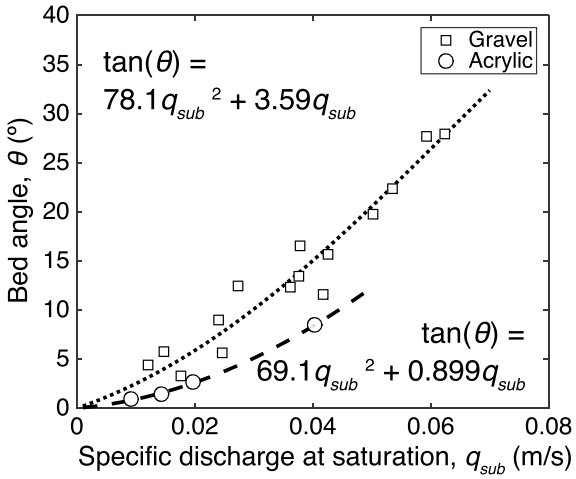

Figure 3. Bed angle as a function of measured specific discharge of subsurface flow. The best fit second-degree polynomial to measured discharges for the natural gravel (dashed line) and acrylic (dotted line) are those used in calculating the saturated subsurface discharge for all slopes (equations shown in the upper left and lower right corners, respectively).

the air-water interface at a subsaturated level between 7 and 9 cm and extrapolated the discharge (measured using a flow meter) linearly to the full bed thickness (10.5 cm). These measured values were averaged for each slope. Due to high subsurface Reynolds numbers ($Re_s = 250$ to 700), our observed specific discharges followed a Forchheimer curve rather than Darcy's law for natural gravel and acrylic, respectively,

$$\tan\theta = 3.59q_{\text{sub}} + 78.1q_{\text{sub}}^2 \quad (5)$$

and

$$\tan\theta = 0.899q_{\text{sub}} + 69.1q_{\text{sub}}^2, \quad (6)$$

where q_{sub} (m/s) is the specific discharge through the sediment bed [*Forchheimer*, 1901] (Figure 3). Equations (5) and (6) were used for the calculation of saturation discharge at all slopes. We measured surface flow velocity by introducing a red dye pulse at the flume inlet and tracking the dye front over a 2.6 m section of the flume using overhead videos recorded from a camera-oriented orthogonal to the water surface at 30 frames per second. We tracked the dye front rather than the dye peak because significant hyporheic exchange slowed the velocity of the dye peak relative to the mean flow velocity. Velocity is assumed to be constant across the channel width, which is true for the initial planar bed. If bed topography develops and the flow becomes confined, this method overpredicts flow velocity and underpredicts flow depth. Accordingly, data collected during the final discharges of some experiments were not used due to the presence of flow confinement.

In calculating flow depth using conservation of mass there are several potential sources of error. These include error in the partitioning of surface and subsurface discharge, error in the measurement of total discharge, and error in the velocity measurement. A maximum error associated with approximating the mean flow velocity by measuring the velocity of the dye front was assessed by comparing measured velocities of the dye front and dye peak, which were typically within 10% of each other. Through repeated calibration of the flowmeter throughout the experiments, errors in the measurement of total discharge were found to typically be less than 3%. Errors in calculating the subsurface discharge were conducted by comparing the depths calculated using conservation of mass to depths measured by mapping the bed surface and water surface in side-view photographs for select experiments (e.g., Figure 1). A direct comparison between flow depths measured using both methods for five bed angles between $\theta = 5.6°$ and 19.6° indicates that the errors in flow depth are typically less than 30%. Consequently, a maximum measurement error of ±30% for flow depth, H, is assumed in our presentation of the experimental results (section 3).

We measured sediment flux for 1 to 10 min at each flow discharge using a sediment trap at the end of the flume (Figure 2). For most experiments we found the critical Shields stress by interpolating the bed load measurements to a reference nondimensional transport rate of $q_b^* = \frac{q_b}{\sqrt{RgDD}} = 2\times10^{-4}$, where q_b is the bed load transport rate per unit channel width [e.g., *Parker et al.*, 1982] (Figure 4). The only exception was the steepest case tested for both the natural gravel and acrylic (22.3° and 2.6°, respectively), which exhibited bed failure in addition to low rates of fluvial transport [e.g., *Prancevic et al.*, 2014]. While fluvial transport was observed in these experiments, subsequent failure of the bed prevented the construction of a power law correlation between bed load transport rate and Shields stress (e.g., Figure 4). In these experiments, the flow conditions at the time of bed failure were taken as critical.

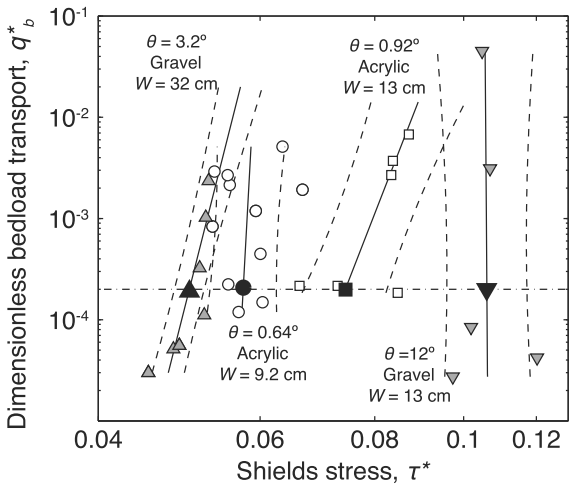

Figure 4. Dimensionless bed load transport as a function of Shields stress for several example experiments with different slopes. Data for both the acrylic (circle and square) and natural (shaded triangle and inverted triangle) gravel experiments are shown. Solid lines are power law fits, and subparallel dotted lines represent 50% confidence limits. Critical Shields stress for each slope is defined at a standard reference dimensionless sediment flux, $q_b^* = 0.0002$ (horizontal dashed line) [*Parker et al.*, 1982].

2.3. Model Comparison

We compared the results with existing models for initial motion of bed sediment [*Wiberg and Smith*, 1987; *Lamb et al.*, 2008; *Recking*, 2009; *Parker et al.*, 2011; *Ferguson*, 2012], which required inputs of grain pocket friction angles, ϕ. ϕ was measured for both the natural gravel (ϕ_g) and acrylic particles (ϕ_a) using tilt table experiments in which a single grain was placed on a planar bed of the same material glued to a board and tilted until the grain dislodged [e.g., *Miller and Byrne*, 1966]. The mean and standard deviation of these angles were $\phi_g = 58.8° \pm 13.7°$ ($n = 296$) and $\phi_a = 40.8° \pm 7.1°$ ($n = 100$).

The *Wiberg and Smith* [1987] model balances driving and resisting forces acting on individual grains to calculate the threshold stress required for motion. However, it was designed for application to relatively deep, low-sloping rivers and includes no components to account for hydraulic changes in steep, shallow flows. The *Lamb et al.* [2008] model builds on that of Wiberg and Smith by including components that account for particle emergence from the flow (reducing buoyancy and the cross-sectional area experiencing drag force), reduced turbulence intensity, and a quadratic (instead of logarithmic) velocity profile within the grain layer. The *Recking* [2009] and *Ferguson* [2012] models instead rely on observations of C_f, and its dependence on relative roughness to predict sediment motion. The Recking model uses flow resistance data to predict an average flow velocity around a sediment grain and also considers the effects of particle emergence. The Ferguson model theorizes that excess flow resistance in shallow flows dissipates the stress available for sediment transport, requiring larger flow depths for incipient motion. We also assess the viability of a constant critical stream power for predicting the onset of sediment transport [e.g., *Ferguson*, 2005; *Parker et al.*, 2011]. Comparing each of these models with our experimental observations allows us to assess their applicability and the validity of the underlying mechanisms.

3. Results

3.1. Shields Stress

Scatter exists in the bed load transport curves (Figure 4) due to both the stochasticity of sediment transport rates and the sources of measurement error discussed in section 2.2. For most of our experiments the sediment flux increased nonlinearly with increased Shields stress, and a fairly wide range of bed load transport rates was observed for a narrow range in Shields stresses (Figure 4). The measured Shields stresses in our experiments varied more so with channel slope than they did with bed load flux at a given slope (Figure 4), and results show a trend of increasing critical Shields stress with increasing bed slope (Figure 5). The error bars in Figures 5 to 9 reflect either the 50% confidence intervals of the best fit bed load curves displayed in Figure 4 or the ±30% uncertainty in the depth measurements (section 2.2), whichever is larger.

Results from the smooth-walled gravel experiments show that τ_c^* increases dramatically from 0.036 at $\theta = 1.9°$ to a maximum value of $\tau_c^* = 0.21$ at $\theta = 22.3°$. Results are similar for the gravel experiments for both channel widths, and for the experiments with rough walls, suggesting that we successfully eliminated effects from particle jamming on initial motion within error (Figure 5). Results of the acrylic experiments are strikingly different from those of the gravel experiments. For example, at the same bed slope of about 2°, τ_c^* for the

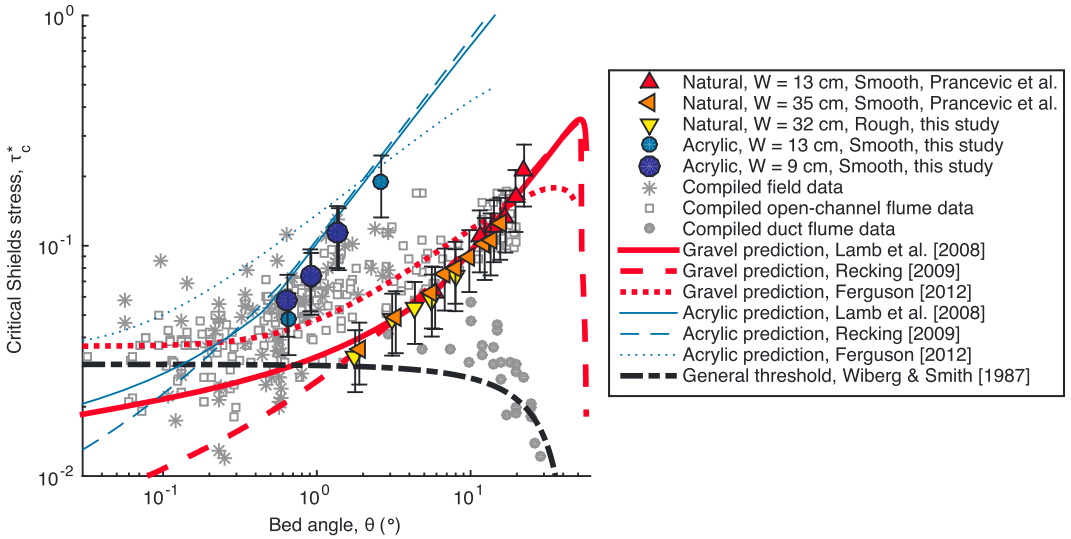

Figure 5. The critical Shields stress as a function of bed angle for all experimental results (solid symbols), model predictions (dotted, dashed, and solid lines), and data compilation (grey asterisks are field observations from the Buffington et al. compilation with $Re_p > 10^2$ [*Buffington and Montgomery*, 1997] and subsequent studies [*Mueller et al.*, 2005], open squares are open channel flume measurements from the Buffington et al. compilation with $Re_p > 10^2$ [*Buffington and Montgomery*, 1997] and subsequent studies [*Shvidchenko and Pender*, 2000; *Gregoretti*, 2008], and grey circles are sealed duct flume measurements [*Fernandez Luque and Van Beek*, 1976; *Chiew and Parker*, 1994; *Dey and Debnath*, 2000]). "Rough" refers to those experiments that had a fixed layer of gravel on each wall. All other experiments had walls of smooth acrylic and epoxy-covered wood. The error bars represent ±30% measurement error or confidence limits calculated from bed load curves (e.g., Figure 4). The model of *Wiberg and Smith* [1987] makes the same prediction for acrylic and gravel.

acrylic data are approximately a factor of 3 larger than for the gravel (Figure 5). Like the gravel experiments, changing channel width had no effect on initial sediment motion in the acrylic experiments, such that enhanced particle jamming cannot explain the offset between the gravel and acrylic data sets. Furthermore, at low slopes the acrylic experiments had subcritical Froude numbers, whereas the gravel had supercritical

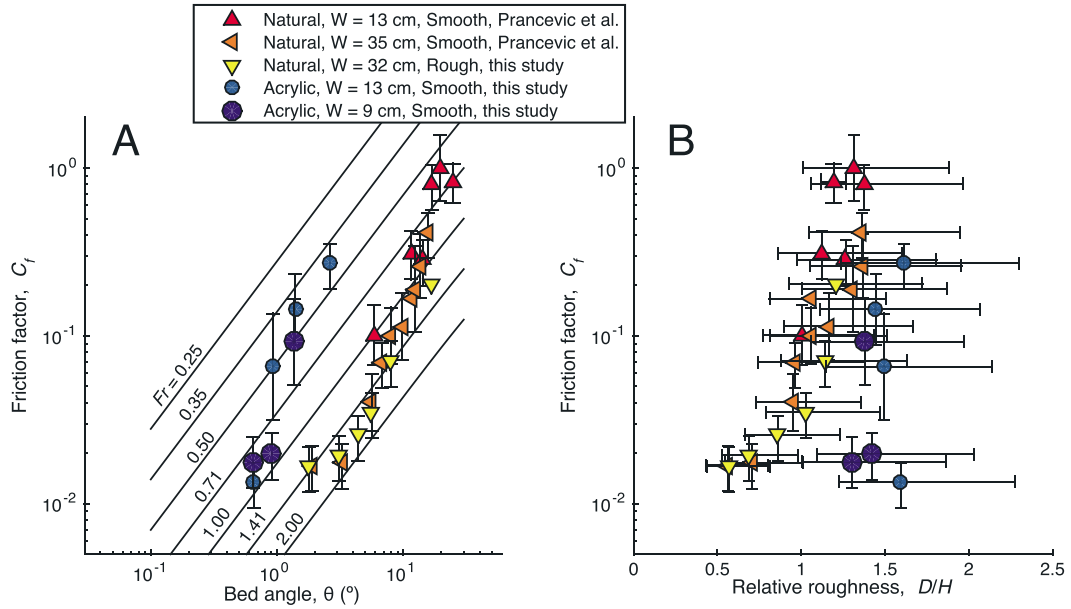

Figure 6. (a) Friction factor at the onset of motion as a function of bed slope for all experimental results. The parallel solid black lines are constant Froude numbers calculated by assuming steady, uniform flow and substituting $u^* = \sqrt{gH \sin\theta}$ and $U = Fr\sqrt{gH}$ into equation (2). (b) Friction factor as a function of relative roughness for all experimental data. The error bars indicate ±30% measurement error or bed load confidence limits (e.g., Figure 4).

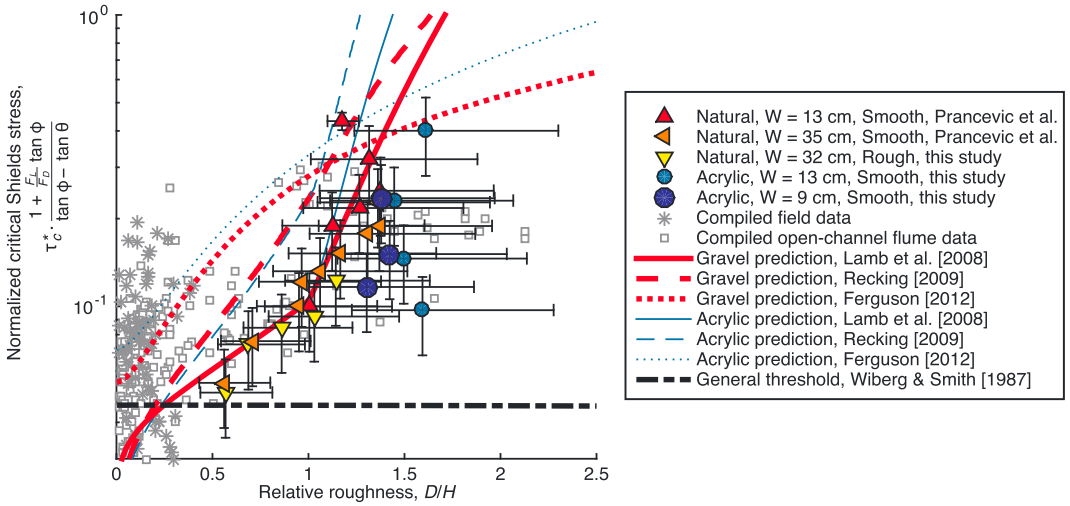

Figure 7. The critical Shields stress as a function of relative roughness for the same data shown in Figure 5. The sealed duct data are not included because relative roughness is not meaningful without a free surface. Note the similar trend and distribution of data to C_f versus D/H (Figure 6b). The error bars represent ±30% measurement error or bed load confidence limits (e.g., Figure 4).

Froude numbers (Figure 6a), which is opposite to the expected trend if the heightened critical Shields stresses for the acrylic were due to $Fr > 1$. Instead, the observed difference in Froude number is likely a secondary effect of increased frictional resistance as flow depth shallows relative to grain size (Figure 6b), causing anomalously slow velocities in the shallow and low-sloping acrylic experiments. This increased frictional resistance is expected for flows with increasing D/H [e.g., *Bathurst*, 1985; *Grant*, 1997].

The effect of relative roughness (independent of channel slope) may be further evaluated by recasting τ_c^* as a function of D/H using equation (4). The natural gravel and the acrylic particles exhibit substantially different particle friction angles ($\phi_g = 58.8°$ and $\phi_a = 40.8°$). Moreover, the steeper bed angles at which the gravel experiments were conducted increase the downstream component of gravity acting on the grains, relative to the acrylic experiments. In order to remove the gravitational and particle friction effects, all data were normalized by the friction angle and bed angle term in the force balance models: $\frac{\tan\varphi - \tan\theta}{1 + F_L/F_D \tan\phi}$, where $F_L/F_D = 0.85$ is the assumed ratio of lift and drag forces acting on the grains [e.g., *Wiberg and Smith*, 1987; *Lamb et al.*, 2008; *Recking*, 2009] (Figure 7). In this space the gravel and acrylic data sets nearly collapse to the same trend. Results for the gravel show increasing τ_c^* with increasing relative roughness, with a significant increase in the slope of this trend for $D > H$ corresponding to either where particles are partially emergent from the flow or where water cascades over the particle tops (Figure 1). The data trend is similar to that shown in a compilation by *Bettess* [1984] using gravel of uniform density, but they investigated only $D/H < 1$. For a given value of relative roughness (e.g., $D/H = 1.4$), the acrylic data appear to have slightly smaller τ_c^* values than the gravel. These differences must be due to factors besides relative roughness that may include altered hydraulics at different slopes. For example, for $D/H = 1.4$ the gravel experiments were at much steeper bed slopes ($14° < \theta < 16°$) than the acrylic ($0.92° < \theta < 1.3°$), resulting in increased flow spilling over grains. Despite these major differences in slope, the near collapse of the acrylic and gravel data in Figure 7, as compared with Figure 5, shows that relative roughness was the key parameter controlling initial sediment motion in our experiments, not bed slope.

The experimental data are in general agreement with the model predictions of *Lamb et al.* [2008] and *Recking* [2009] for the natural gravel and acrylic particles (Figures 5 and 7), although τ_c^* for the acrylic particles is overpredicted. The *Ferguson* [2012] model captures the general trends but overpredicts the Shields stress required to transport both materials. In contrast, the model of *Wiberg and Smith* [1987], which does not include relative roughness as a factor, shows decreasing τ_c^* with increasing slope and is consistent only with sealed duct experiments where D/H does not vary with slope (Figure 5).

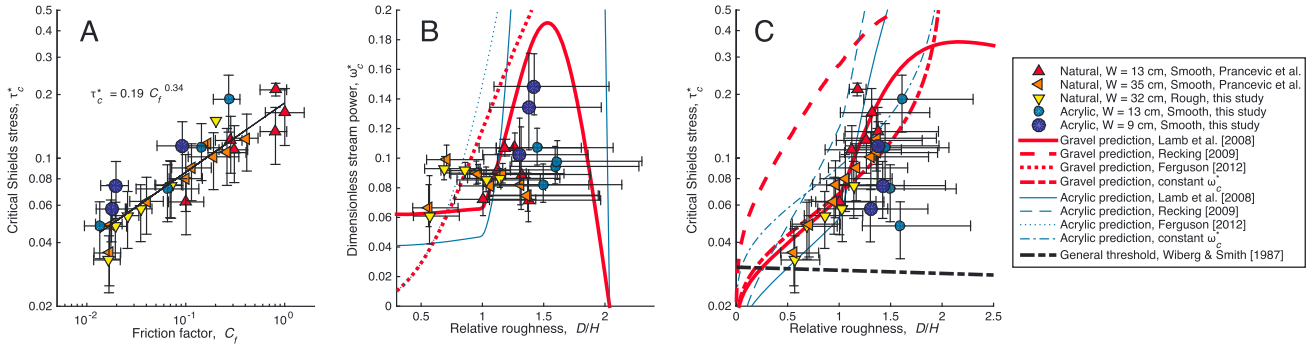

Figure 8. (a) Friction factor as a function of critical Shields stress for both materials and a best fit power law relating the two parameters. (b) Critical dimensionless unit stream power (equation (3)) as a function of relative roughness. The *Lamb et al.* [2008] Shields stress model has been recast to solve for the critical stream power using equations (7) and (8). (c) The critical Shields stress (uncorrected for slope and friction angle differences) as a function of relative roughness. The *Lamb et al.* [2008] and *Recking* [2009] models are shown, as well as the critical Shields stress predicted by a constant critical stream power and equations (7) and (8). The error bars represent ±30% measurement error or bed load confidence limits (e.g., Figure 4).

3.2. Flow Resistance and Stream Power

In our experiments, flow resistance (C_f) at the onset of sediment motion exhibits a similar increase with D/H to the Shields stress (compare Figure 6b to Figure 7). The steep increase in flow resistance with relative roughness has been documented previously [*Bathurst*, 1985; *Rickenmann and Recking*, 2011; *Ferguson*, 2012], but the offset in flow resistance between acrylic and gravel data sets for a given relative roughness indicates that there may be an additional bed slope dependence, such as spilling around and over particles. Despite this potential slope effect, a strong power law relationship exists between Shields stress and flow resistance (Figure 8a). Under the assumption of steady and uniform flow, and using equations (1)–(3), critical stream power can be rewritten as follows:

$$\omega_c^* = \left(\frac{\tau_c^*}{C_f^{1/3}}\right)^{3/2}. \tag{7}$$

Equation (7) shows that if ω_c^* is constant, then critical Shields stress must be proportional to flow resistance to the one-third power, consistent with our observations (Figure 8a). The acrylic experiments show higher values for critical stream power (Figure 8b), but the data generally cluster around an average of $\omega_c^* = 0.11$ for the acrylic and $\omega_c^* = 0.085$ for the natural gravel, similar to the data compilation of *Parker et al.* [2011].

To compare these experimental observations to theoretical expectations of critical stream power, we employ equation (7) and predicted values of C_f and τ_c^*. Here we use the established flow resistance relationship of *Bathurst* [1985]:

$$C_f^{-1/2} = 5.62 \log\left(\frac{H}{D_{84}}\right) + 4 \tag{8}$$

and the critical Shields stress model of *Lamb et al.* [2008] to predict a critical stream power (Figure 8b). For comparison, *Ferguson's* [2012] model is also shown in Figure 8b and uses the variable-power flow resistance equation of *Ferguson* [2007]. The Lamb-Bathurst model for critical stream power predicts near-constant values for $D/H \leq 1$, similar to our experimental observations. For shallower flows ($D/H > 1$), the predicted stream power values increase sharply and diverge from observations. The Ferguson model predicts a steep relationship between ω_c^* and D/H for all values tested, diverging from most of our experimental data. The divergence of our experimental observations with these model predictions occurs because the predicted values of C_f and τ_c^* do not maintain the same one-third-power covariance as we observe in our experimental data.

In a similar inversion, we may recast a constant stream power value ($\omega_c^* = 0.085$ for the natural gravel and $\omega_c^* = 0.11$ for the acrylic) as a critical Shields stress using equations (7) and (8) (Figure 8c). The Shields stresses predicted using this method are within error of measurements in the gravel experiments, with a

slight underestimation for the very steep and shallow experiments ($D/H > 1$). Similar to the *Lamb et al*. [2008] model, the stream power inversion overestimates critical Shields stresses for the acrylic experiments, but to a lesser degree.

4. Discussion

4.1. The Effects of Flow Depth, Slope, Form Drag, and Jamming on Incipient Motion

The only variables that differ significantly between the gravel and the acrylic experiments at a given channel slope are submerged specific particle density (R) and relative roughness (D/H). The effect of submerged specific density on particle weight, however, is already accounted for in the definition of the critical Shields stress (equation (1)) [i.e., *Archimedes*, 1897], such that in the absence of relative roughness effects, the acrylic and gravel data sets should collapse to a similar trend. They do not. Therefore, the systematic offset of the acrylic data to higher τ_c^* at a given channel slope is due to the effect of increased relative roughness alone. This is the first conclusive evidence to show that increased relative roughness alone can cause heightened τ_c^* in the absence of steep channel slopes, form drag induced by bed forms, particle jamming or interlocking caused by narrow channel widths, relative grain size, or supercritical Froude numbers. This notwithstanding, many of the compiled field data (Figure 5) exhibit critical Shields stresses that are larger than our experimental results for a given channel slope. This discrepancy is likely due to other factors that were purposefully eliminated in our experiments including particle jamming and interlocking and form drag from bed forms [*Zimmermann and Church*, 2001; *Yager et al*., 2007; *Zimmermann et al*., 2010]. In natural channels, relative roughness, bed forms, and particle jamming may be intertwined. For example, roughness due to bed forms is larger than that due to grains, and therefore, bed forms may also induce larger τ_c^* through changes in relative roughness, in addition to changes in morphologic form drag.

Although we have shown that relative roughness has a profound impact on sediment mobility, the slight offset between the acrylic and gravel data in plots of Shields stress (Figure 7), flow resistance (Figure 6b), and stream power (Figure 8b) versus D/H indicates that there may be an additional bed slope effect on these parameters that has not previously been recognized. Because C_f is a hydraulic parameter it does not depend on the material density of the grains, and a significant offset between the gravel and acrylic data should not exist. The slight offset that is present may suggest that the steeper slopes tested in the gravel experiments induced higher flow resistance. Alternatively, this offset may be due to differences in particle shape and texture (e.g., Figure 1). Regardless of the cause in the offset of C_f between the two materials, the reduced flow velocities of the gravel experiments relative to the acrylic, for a given relative roughness, appear to have affected the conditions required for sediment transport. For example, the slight offset observed in τ_c^* versus D/H (Figure 7) may be explained by slower local flow velocities and reduced turbulent intensity around the gravel relative to the acrylic. Conversely, multiplying the critical shear stress by heightened flow velocities in the acrylic experiments boosts the stream power required for transport relative to the gravel in ω_c^* versus D/H (Figure 8b).

4.2. Assessment of Models

4.2.1. Predicted Critical Shields Stress

Our results are consistent with models that consider the effects of relative roughness on flow hydraulics and near-bed turbulence [*Lamb et al*., 2008; *Recking*, 2009], and inconsistent with models that do not consider these effects [*Wiberg and Smith*, 1987]. The *Ferguson* [2012] model overpredicts the critical Shields stress for most of our experimental conditions (Figure 5). The Ferguson model is less mechanistic by design and performs considerably well due to the interrelated nature of flow resistance, Shields stress, and stream power. However, it lacks predictive power where the flow resistance is not known or data is scarce, such as slopes greater than ~10° [e.g., *Comiti et al*., 2007]. The models of *Lamb et al*. [2008] and *Recking* [2009] rely on flow resistance models as well but use them to calibrate physical mechanisms that are expected to change with slope and relative roughness, including the mean velocity profile and turbulence intensity. This mechanistic approach ultimately results in improved fits to our experimental data.

Using our experimental observations we can provide some assessment of the mechanisms employed by the models of *Lamb et al*. [2008] and *Recking* [2009]. One mechanism that was violated in some cases was the expectation for particles to emerge from the flow when $D/H > 1$, which would increase the effective particle weight. Even in flows that were on average much shallower than the grain size, most particles remained submerged by flow traveling up and over the grain (Figure 1). However, calculating buoyancy, lift, and drag

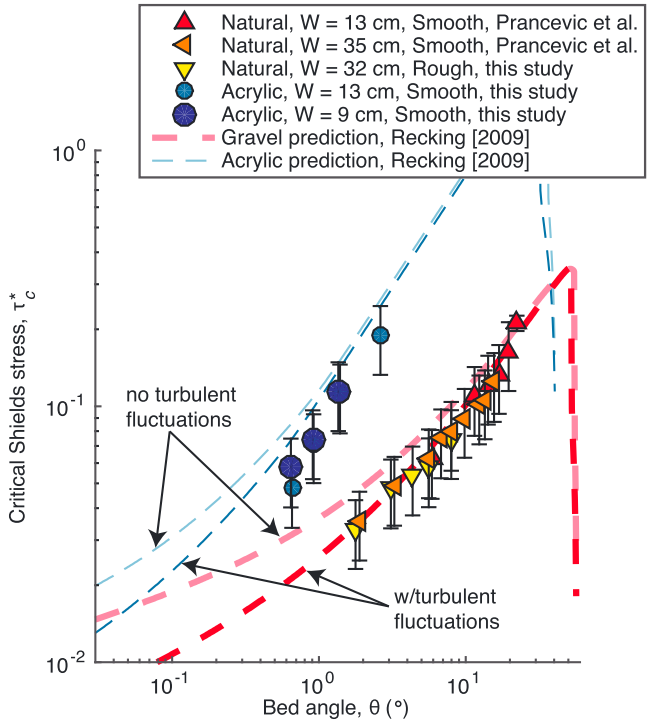

Figure 9. Critical Shields stress of experimental data and the *Recking* [2009] model versus bed angle. The original Recking model (light lines) for both materials does not include the effect of reduced turbulence intensity in shallow flows, but the modified version (bold lines) does. The error bars represent 50% confidence limits calculated from bed load curves.

forces within such cascading flow is not straightforward, as fine-scale velocity and pressure measurements in rough flows are not available.

One way the *Lamb et al.* [2008] and *Recking* [2009] models differ is that the Lamb et al. model includes changing intensity of turbulence fluctuations with relative roughness, in addition to changes in mean flow velocity. Specifically, *Lamb et al.* [2008] propose that the transport-inducing drag force bearing on a grain, F_D, is not simply a function of local flow velocity (i.e., $F_D \propto u^2(z)$), but it has an additional dependence on the depth-averaged velocity:

$$F_D \propto \left\langle (u(z) + \alpha U)^2 \right\rangle, \quad (9)$$

where $\alpha \approx 0.2$ is a constant relating U to the magnitude of turbulent fluctuations near the bed and the brackets indicate spatial averaging over the submerged height of the grain. As discussed in the next section (4.2.2), the use of a depth-averaged flow velocity term is supported both by the fit of the Lamb et al. model and reduced variability observed in our measured values of critical stream power. Indeed, adding the turbulent component to the Recking model improves its fit with our experimental observations as well (Figure 9), suggesting that reduced turbulence intensity in shallow flows plays an important role in increasing the critical Shields stress for sediment transport.

4.2.2. Constant Critical Stream Power

A constant critical stream power predicts the onset of sediment motion within error for most experiments within a given experiment set. This collapse of the experimental data to a small range in critical stream power values indicates that multiplying the Shields stress by the respective depth-averaged flow velocity greatly reduces variability after normalizing for grain weight (e.g., equation (3)). This additional velocity term may be mechanistically justified. In the development of their Shields stress model, *Lamb et al.* [2008] propose that the magnitude of turbulent fluctuations scales with the depth-averaged flow velocity (equation (9)). The additional velocity term used to calculate the drag force does not yield an equation of the same form as stream power, but it does produce a critical Shields stress that depends on the depth-averaged flow velocity, providing some grain-scale justification for a constant critical stream power model.

However, offsets exist between the gravel and acrylic experiments and between the data sets compiled by *Parker et al.* [2011]. This variability indicates that a single value of critical stream power cannot be universally applied. Moreover, the variability of critical stream power is not easily predicted because a grain-scale model that relates stream power directly to energy acting on grains has not been established. Instead, stream power models like the one presented in section 3.2 rely on physically based predictions of critical shear stress that are subsequently multiplied by predicted mean flow velocities [e.g., *Parker et al.*, 2011; *Ferguson*, 2012]. As a result, critical stream power predictions to date account for changes in bed conditions (e.g., particle friction angle and relative grain size) only by utilizing models for critical shear stress.

4.3. Implications for Bed Load Transport Rates

Measured bed load transport rates in steep mountain channels are commonly an order of magnitude smaller than predicted by traditional bed load transport formulas developed for lower sloping rivers [e.g., *Rickenmann*, 2001; *Mueller et al*., 2008; *Nitsche et al*., 2011; *Yager et al*., 2012]. These transport equations often have the general form:

$$q_b^* = a\left(\tau^* - \tau_c^*\right)^b, \tag{10}$$

where a and b are empirical constants that vary from $a = 4.9$ to 8.0 and $b = 1.5$ to 1.6 [e.g., *Meyer-Peter and Mueller*, 1948; *Fernandez Luque and Van Beek*, 1976; *Wong and Parker*, 2006]. Equation (10) may be modified in several ways to provide a better prediction in steep channels: a and b may be adjusted to smaller values, τ_c^* may be increased, and τ^* may be replaced with a reduced "effective" Shields stress that is available to transport sediment. The latter approach is most commonly favored and is typically conceptualized as momentum spent on morphologic form drag due to large immobile boulders, step-pools, or other bed forms [e.g., *Rickenmann*, 2001; *Yager et al*., 2007].

Our results indicate that τ_c^* increases with channel bed slope, which according to equation (10) should reduce bed load transport rates even in the absence of form drag from immobile obstacles or bed forms. In addition, the hydraulic mechanisms of reduced near-bed mean flow velocities and turbulent intensity in rivers with high relative roughness are not limited to the onset of sediment motion. These mechanisms should be important in reducing the expected bed load flux at all transport stages. Indeed, a recent study that evaluated sediment transport models at 13 steep mountain streams found that the best fit formulas use both an increased critical Shields stress (τ_c^*) and a reduced effective Shields stress available to transport sediment (τ^*) [*Nitsche et al*., 2011]. Although Nitsche et al. attribute the decrease in effective Shields stress to morphologic form drag from bed forms, our results suggest that effective Shields stress can be lower than expected in steep mountain streams even with a planar bed because of changes in near-bed hydraulics associated with high relative roughness.

4.4. Sediment Density and Incipient Motion

In addition to the usefulness of changing density to isolate relative roughness from channel slope, our results have direct application to sediment transport of particles of different densities. These cases are relatively rare on Earth, but some prominent examples exist elsewhere. For example, on Titan, liquid hydrocarbons (e.g., ethane and methane) are thought to transport clasts of water ice and solid organic particles, yielding a relative submerged density range of $R = 0.5$ to 2 [*Perron et al*., 2006; *Lorenz et al*., 2010; *Grotzinger et al*., 2013]. On a relatively low bed angle of $\theta = 0.1°$, this density range yields a critical Shields stress range of $\tau_c^* = 0.021$ to 0.026 according to the *Lamb et al*. [2008] model. On a steeper slope of $\theta = 5°$, the range in predicted Shields stresses widens considerably to $\tau_c^* = 0.054$ to 0.14 due to the enhanced effects of large D/H for different particle densities. On Mars, the transportation of basalt-derived sediment by liquid water ($R = 1.65$ for plagioclase and $R = 1.9$ for intact basalt) should yield similar Shields stresses to those observed on Earth [e.g., *Grotzinger et al*., 2013]. However, transport by high-density brines ($R = 1.04$) requires heightened Shields stresses for channels with the same bed slope [*Tosca et al*., 2011; *Lamb et al*., 2012]. For example, on a steep slope of $\theta = 5°$, the increase in density from freshwater to dense brine should increase the critical Shields stress from 0.059 to 0.080. On Earth, differences in sediment density are typically small, with a few rare exceptions (e.g., pumice, and iron oxides and sulfides [e.g., *Johnson et al*., 2014]). Still, the increased density between granitic clasts ($R = 1.65$) and intact basalt ($R = 1.9$) should cause a decrease of the critical Shields stress on the order of 10% in steep channels ($\theta \geq 5°$), which is of similar magnitude as other factors affecting gravel mobility, such as the addition of 15% sand to a gravel sediment mixture [e.g., *Wilcock et al*., 2001]. The variability of the critical Shields stress that is associated with relative submerged density indicates that sediment transport calculations should be performed in a material-specific manner, particularly on steep slopes and with exotic materials.

5. Conclusions

By performing flume experiments with both gravel ($R = 1.65$) and acrylic ($R = 0.15$) grains we were able to separate the relative roles of bed angle, θ, and relative roughness, D/H, in affecting the critical Shields stress required for sediment transport in open-channel flows. Both materials exhibited a sharp increase in the

Shields stress at the onset of motion with increasing bed slope. For the same bed slope, the Shields stress required to mobilize the lighter acrylic material was roughly threefold larger than the gravel. Controls on bed form development and channel width indicate that the offset between our acrylic and gravel data sets is due mostly to differences in D/H at the onset of motion. Measurements of flow resistance in the same experiments confirm a strong dependence of flow resistance on D/H. A slight offset to higher flow resistance for the gravel experiments may be responsible for the higher critical Shields stresses for the gravel compared to the acrylic for a given value of relative roughness, owing to the slower velocities around the gravel grains than the acrylic grains.

The models of *Lamb et al*. [2008] and *Recking* [2009] are best suited to predict the critical Shields stress observed in our experiments because they explicitly account for particle emergence and altered velocity profiles in shallow flows. The Lamb et al. model provides a slightly better fit by including an additional component to account for reduced intensity of turbulent fluctuations in shallow flows. Adding this component to the Recking model improved that fit as well.

Although the critical Shields stress for sediment motion was observed to increase with bed slope, the stream power at the onset of motion remained relatively constant for a given material. Variability in the critical stream power values between experiment sets, however, indicates that a single value is not appropriate for all channel conditions and mechanistic explanations are not readily available. This notwithstanding, the consistency of critical stream power at the onset of motion in this study and others is encouraging for large-scale landscape evolution modeling [e.g., *Howard*, 1994; *Tucker and Slingerland*, 1997; *Lague*, 2003; *Dibiase and Whipple*, 2011], which relies on parameterizing stream power using drainage area and slope.

Our results indicate that there exists no universal trend for τ_c^* with channel slope and instead that τ_c^* is a function of relative roughness, which can vary substantially with bed slope and with particle density. Moreover, the heightened critical Shields stress observed in our experiments, in which we controlled for bed forms and particle interlocking, represent baseline values that may be further augmented in natural shallow channels by morphologic form drag and particle interlocking. These relative roughness effects help to explain reduced bed load fluxes in steep channels. Our results are also important for reconstructing flow conditions on other planets, for example, where initial sediment motion of ice clasts has been used to constrain methane precipitation rates on Titan [*Perron et al*., 2006], or where transport of evaporite grains have been used to constrain flow rates of brines on Mars [*Lamb et al*., 2012].

Notation

C_f	friction factor
D	length of the intermediate axis of the median grain size (D_{50})
D_n	nth percentile grain diameter
F_D	drag force
F_L	lift force
Fr	Froude number
g	gravitational acceleration
H	flow depth
q_{surf}	surface discharge per unit width
q_{sub}	specific discharge of subsurface flow
R	relative submerged density of sediment
Re_p	particle Reynolds number
Re_s	subsurface Reynolds number
U	mean flow velocity
U	local flow velocity
u^*	shear velocity
W	channel width
α	turbulent fluctuation coefficient
θ	bed angle
ρ	density of water
ρ_s	material density of sediment

τ_b total bed shear stress
τ^* Shields stress
τ_c^* Shields stress at the onset of motion
τ_{eff}^* effective Shields stress
ϕ_g particle friction angle of natural gravel
ϕ_a particle friction angle of deformed acrylic spheres
ω stream power per unit width
ω_c^* nondimensional stream power per unit width at the onset of motion

Acknowledgments
Funding was provided by NSF grants EAR-0922199 and EAR-1349115, the Terrestrial Hazards Observations and Reporting center (THOR) at Caltech, and the Keck Institute for Space Studies. The experimental data presented in Figures 5 to 9 are either present in Table 1 or may be calculated from data in Table 1 using equations included in the manuscript. We thank Brian Fuller for help with experiments. This paper was improved by the helpful comments of two anonymous reviewers.

References

Aksoy, S. (1973), The influence of the relative depth on threshold of grain motion, in *Proceedings of the International Association for Hydraulic Research International Symposium on River Mechanics*, pp. 359–370, Int. Assoc. for Hydraul. Res., Delft, Netherlands.
Archimedes (1897), On floating bodies I, in *Works of Archimedes*, edited by T. L. Heath, pp. 258–261, Cambridge Univ. Press, Cambridge.
Ashida, K., and M. Bayazit (1973), Initiation of motion and roughness of flows in steep channels, in *Proceedings of the 15th Congress*, vol. 1, pp. 475–484, Int. Assoc. Hydraul. Res., Istanbul, Turkey.
Bagnold, R. A. (1980), An empirical correlation of bedload transport rates in flumes and natural rivers, *Proc. R. Soc. A*, *372*(1751), 453–473, doi:10.1098/rspa.1980.0122.
Bathurst, J. C. (1985), Flow resistance estimation in mountain rivers, *J. Hydraul. Eng.*, *111*(4), 625–643, doi:10.1061/(ASCE)0733-9429(1985)111:4(625).
Bathurst, J. C., H. H. Cao, and W. H. Graf (1984), Hydraulics and sediment transport in a steep flume: Data from the EPFL study, Report, Centre for Ecology and Hydrology, Wallingford, U. K.
Bayazit, M. (1976), Free surface flow in a channel of large relative roughness, *J. Hydraul. Res.*, *14*(2), 115–126, doi:10.1080/00221687609499676.
Bettess, R. (1984), Initiation of sediment transport in gravel streams, *Proc. Inst. Civ. Eng. Part 2*, *77*, 79–88.
Buffington, J. M., and D. R. Montgomery (1997), A systematic analysis of eight decades of incipient motion studies, with special reference to gravel-bedded rivers, *Water Resour. Res.*, *33*(8), 1993–2029, doi:10.1029/96WR03190.
Buffington, J. M., and D. R. Montgomery (1999), Effects of sediment supply on surface textures of gravel-bed rivers, *Water Resour. Res.*, *35*(11), 3523–3530, doi:10.1029/1999WR900232.
Bunte, K., S. R. Abt, K. W. Swingle, D. A. Cenderelli, and J. M. Schneider (2013), Critical Shields values in coarse-bedded steep streams, *Water Resour. Res.*, *49*, 7427–7447, doi:10.1002/2012WR012672.
Carollo, F., V. Ferro, and D. Termini (2005), Analyzing turbulence intensity in gravel bed channels, *J. Hydraul. Eng.*, *131*(12), 1050–1061, doi:10.1061/(ASCE)0733-9429(2005)131:12(1050).
Chiew, Y.-M., and G. Parker (1994), Incipient sediment motion on non-horizontal slopes, *J. Hydraul. Res.*, *32*(5), 649–660, doi:10.1080/00221689409498706.
Comiti, F., L. Mao, A. Wilcox, E. E. Wohl, and M. A. Lenzi (2007), Field-derived relationships for flow velocity and resistance in high-gradient streams, *J. Hydrol.*, *340*(1–2), 48–62, doi:10.1016/j.jhydrol.2007.03.021.
Costa, J. (1983), Paleohydraulic reconstruction of flash-flood peaks from boulder deposits in the Colorado Front Range, *GSA Bull.*, *94*(8), 986–1004, doi:10.1130/0016-7606(1983)94<986:PROFPF>2.0.CO;2.
Dey, S., and K. Debnath (2000), Influence of streamwise bed slope on sediment threshold under stream flow, *J. Irrig. Drain. Eng.*, *126*(4), 255–263, doi:10.1061/(ASCE)0733-9437(2000)126:4(255).
Dibiase, R. A., and K. X. Whipple (2011), The influence of erosion thresholds and runoff variability on the relationships among topography, climate, and erosion rate, *J. Geophys. Res.*, *116*, F04036, doi:10.1029/2011JF002095.
Ferguson, R. I. (2005), Estimating critical stream power for bedload transport calculations in gravel-bed rivers, *Geomorphology*, *70*(1–2), 33–41, doi:10.1016/j.geomorph.2005.03.009.
Ferguson, R. I. (2007), Flow resistance equations for gravel-and boulder-bed streams, *Water Resour. Res.*, *43*, W05427, doi:10.1029/2006WR005422.
Ferguson, R. I. (2012), River channel slope, flow resistance, and gravel entrainment thresholds, *Water Resour. Res.*, *48*, W05517, doi:10.1029/2011WR010850.
Fernandez Luque, R., and R. Van Beek (1976), Erosion and transport of bed-load sediment, *J. Hydraul. Res.*, *14*(2), 127–144.
Flammer, G. H., J. P. Tullis, and E. S. Mason (1970), Free surface, velocity gradient flow past hemisphere, *J. Hydraul. Div.*, *96*(7), 1485–1502.
Forchheimer, P. H. (1901), Wasserbewegun Durch Boden, *Z. Ver. Dtsch. Ing.*, *45*(50), 1781–1788.
Grant, G. E. (1997), Critical flow constrains flow hydraulics in mobile-bed streams: A new hypothesis, *Water Resour. Res.*, *33*(2), 349–358, doi:10.1029/96WR03134.
Gregoretti, C. (2008), Inception sediment transport relationships at high slopes, *J. Hydraul. Eng.*, *134*(11), 1620–1629, doi:10.1061/(ASCE)0733-9429(2008)134:11(1620).
Grotzinger, J. P., A. G. Hayes, M. P. Lamb, and S. M. McLennan (2013), Sedimentary processes on Earth, Mars, Titan, and Venus, *Comp. Climatol. Terr. Planets*, *1*, 439–472.
Hack, J. T. (1957), Studies of longitudinal stream profiles in Virginia and Maryland, U.S. Geol. Surv. Prof. Pap.
Howard, A. D. (1994), A detachment-limited model of drainage basin evolution, *Water Resour. Res.*, *30*(7), 2261–2285, doi:10.1029/94WR00757.
Johnson, J. E., A. Gerpheide, M. P. Lamb, and W. W. Fischer (2014), O2 constraints from Paleoproterozoic detrital pyrite and uraninite, *Geol. Soc. Am. Bull.*, *126*(5–6), 813–830, doi:10.1130/B30949.1.
Kirchner, J. W., W. E. Dietrich, F. Iseya, and H. Ikeda (1990), The variability of critical shear stress, friction angle, and grain protrusion in water-worked sediments, *Sedimentology*, *37*, 647–672, doi:10.1111/j.1365-3091.1990.tb00627.x.
Lague, D. (2003), Constraints on the long-term colluvial erosion law by analyzing slope-area relationships at various tectonic uplift rates in the Siwaliks Hills (Nepal), *J. Geophys. Res.*, *108*(B2), 2129, doi:10.1029/2002JB001893.
Lamb, M. P., W. E. Dietrich, and J. G. Venditti (2008), Is the critical Shields stress for incipient sediment motion dependent on channel-bed slope?, *J. Geophys. Res.*, *113*, F02008, doi:10.1029/2007JF000831.

Lamb, M. P., J. P. Grotzinger, J. B. Southard, and N. J. Tosca (2012), Were aqueous ripples on Mars formed by flowing brines?, in *Sedimentary Geology of Mars*, vol. 102, pp. 139–150, SEPM Special Publication Society for Sedimentary Geology, Tulsa, Okla.

Lorenz, R. D., C. Newman, and J. I. Lunine (2010), Threshold of wave generation on Titan's lakes and seas: Effect of viscosity and implications for Cassini observations, *Icarus*, *207*(2), 932–937, doi:10.1016/j.icarus.2009.12.004.

Meyer-Peter, E., and R. Mueller (1948), Formulas for bed-load transport, in *Proceedings of the 2nd Congress*, Int. Assoc. Hydraul. Res., pp. 39–64, Stockholm, Sweden.

Miller, R. L., and R. J. Byrne (1966), The angle of repose for a single grain on a fixed rough bed, *Sedimentology*, *6*(4), 303–314, doi:10.1111/j.1365-3091.1966.tb01897.x.

Mueller, E. R., J. Pitlick, and J. M. Nelson (2005), Variation in the reference Shields stress for bed load transport in gravel-bed streams and rivers, *Water Resour. Res.*, *41*, W04006, doi:10.1029/2004WR003692.

Mueller, E. N., R. J. Batalla, C. Garcia, and A. Bronstert (2008), Modeling bed-load rates from fine grain-size patches during small floods in a gravel-bed river, *J. Hydraul. Eng.*, *134*(10), 1430–1439, doi:10.1061/(ASCE)0733-9429(2008)134:10(1430).

Nikora, V., D. Goring, I. McEwan, and G. Griffiths (2001), Spatially averaged open-channel flow over rough bed, *J. Hydraul. Eng.*, *127*(2), 123–133, doi:10.1061/(ASCE)0733-9429(2001)127:2(123).

Nitsche, M., D. Rickenmann, J. M. Turowski, A. Badoux, and J. W. Kirchner (2011), Evaluation of bedload transport predictions using flow resistance equations to account for macro-roughness in steep mountain streams, *Water Resour. Res.*, *47*, W08513, doi:10.1029/2011WR010645.

Parker, G., P. C. Klingeman, and D. G. McLean (1982), Bedload and size distribution in paved gravel-bed streams, *J. Hydraul. Div.*, *108*(4), 544–571.

Parker, C., N. J. Clifford, and C. R. Thorne (2011), Understanding the influence of slope on the threshold of coarse grain motion: Revisiting critical stream power, *Geomorphology*, *126*(1–2), 51–65, doi:10.1016/j.geomorph.2010.10.027.

Perron, J. T., M. P. Lamb, C. D. Koven, I. Y. Fung, E. Yager, and M. Ádámkovics (2006), Valley formation and methane precipitation rates on Titan, *J. Geophys. Res.*, *111*, E11001, doi:10.1029/2005JE002602.

Prancevic, J. P., M. P. Lamb, and B. M. Fuller (2014), Incipient sediment motion across the river to debris-flow transition, *Geology*, *42*, 191–194, doi:10.1130/G34927.1.

Recking, A. (2009), Theoretical development on the effects of changing flow hydraulics on incipient bed load motion, *Water Resour. Res.*, *45*, W04401, doi:10.1029/2008WR006826.

Rickenmann, D. (2001), Comparison of bed load transport in torrents and gravel bed streams, *Water Resour. Res.*, *37*(12), 3295–3305, doi:10.1029/2001WR000319.

Rickenmann, D., and A. Recking (2011), Evaluation of flow resistance in gravel-bed rivers through a large field data set, *Water Resour. Res.*, *47*, W07538, doi:10.1029/2010WR009793.

Scheingross, J. S., E. W. Winchell, M. P. Lamb, and W. E. Dietrich (2013), Influence of bed patchiness, slope, grain hiding, and form drag on gravel mobilization in very steep streams, *J. Geophys. Res. Earth Surf.*, *118*, 1–20, doi:10.1002/jgrf.20067.

Shields, A. (1936), *Anwendung der Ähnlichkeitsmechanik und der Turbulenzforschung auf die Geschiebebewegung*, vol. 26, Mitt. Preuss Versuchsanst. Wasserbau Schiffbau, Berlin.

Shvidchenko, A. B., and G. Pender (2000), Flume study of the effect of relative depth on the incipient motion of coarse uniform sediments, *Water Resour. Res.*, *36*(2), 619–628, doi:10.1029/1999WR900312.

Tosca, N. J., S. M. McLennan, M. P. Lamb, and J. P. Grotzinger (2011), Physicochemical properties of concentrated Martian surface waters, *J. Geophys. Res.*, *116*, E05004, doi:10.1029/2010JE003700.

Tucker, G. E., and R. Slingerland (1997), Drainage basin responses to climate change, *Water Resour. Res.*, *33*(8), 2031–2047, doi:10.1029/97WR00409.

Vollmer, S., and M. G. Kleinhans (2007), Predicting incipient motion, including the effect of turbulent pressure fluctuations in the bed, *Water Resour. Res.*, *43*, W05410, doi:10.1029/2006WR004919.

Whipple, K. X., and G. E. Tucker (1999), Dynamics of the stream-power river incision model: Implications for height limits of mountain ranges, landscape response timescales, and research needs, *J. Geophys. Res.*, *104*(B8), 17,661–17,674, doi:10.1029/1999JB900120.

White, C. M. (1940), The equilibrium of grains on the bed of a stream, *Proc. R. Soc. London, Ser. A*, *174*(958), 322–338.

Wiberg, P. L., and J. D. Smith (1987), Calculations of the critical shear stress for motion of uniform and heterogeneous sediments, *Water Resour. Res.*, *23*(8), 1471–1480, doi:10.1029/WR023i008p01471.

Wilcock, P. R., S. T. Kenworthy, and J. C. Crowe (2001), Experimental study of the transport of mixed sand and gravel, *Water Resour. Res.*, *37*(12), 3349–3358, doi:10.1029/2001WR000683.

Wong, M., and G. Parker (2006), Reanalysis and correction of bed-load relation of Meyer-Peter and Müller using their own database, *J. Hydraul. Eng.*, *132*(11), 1159–1168.

Yager, E. M., J. W. Kirchner, and W. E. Dietrich (2007), Calculating bed load transport in steep boulder bed channels, *Water Resour. Res.*, *43*, W07418, doi:10.1029/2006WR005432.

Yager, E. M., J. M. Turowski, D. Rickenmann, and B. W. McArdell (2012), Sediment supply, grain protrusion, and bedload transport in mountain streams, *Geophys. Res. Lett.*, *39*, L10402, doi:10.1029/2012GL051654.

Zimmermann, A., and M. Church (2001), Channel morphology, gradient profiles and bed stresses during flood in a step-pool channel, *Geomorphology*, *40*, 311–327, doi:10.1016/S0169-555X(01)00057-5.

Zimmermann, A., M. Church, and M. A. Hassan (2010), Step-pool stability: Testing the jammed state hypothesis, *J. Geophys. Res.*, *115*, F02008, doi:10.1029/2009JF001365.